

Design, fabrication and testing of achromatic elliptical polarizer

XINGZHOU TU,^{1,*} LINAN JIANG,¹ MOHAMMED IBN-ELHAJ,² AND STANLEY PAU¹

¹University of Arizona, College of Optical Sciences, 1630 East University Boulevard, Tucson, Arizona 85721, USA

²Rolic Technologies Ltd., CH-4123 Allschwil, Switzerland

*xtu@optics.arizona.edu

Abstract: A method of designing achromatic elliptical polarizers using a combination of multiple birefringent waveplates is demonstrated. This approach has a simple geometric interpretation and simplifies the problem of designing an achromatic elliptical polarizer to find overlapping arcs on the Poincaré sphere. The technique is applied to the design of achromatic elliptical polarizers for a broadband division-of-focal-plane full-Stokes imaging polarimeter for visible wavelength band ($\lambda = 450\text{nm}$ to 650nm). An achromatic elliptical polarizer sample with a two-layer retarder is fabricated using liquid crystal polymer. The performance of the polarizer sample is measured and compared with the theoretical calculation. For comparison, a superachromatic polarizer design ($\lambda = 400\text{nm}$ to $1\mu\text{m}$) is also presented by using three-layer and four-layer retarder configurations.

© 2017 Optical Society of America

OCIS codes: (120.4570) Optical design of instruments; (120.4610) Optical fabrication; (120.5410) Polarimetry; (230.5440) Polarization-selective devices; (260.5430) Polarization.

References and links

1. P. Hariharan and P. E. Ciddor, "Broad-band superachromatic retarders and circular polarizers for the UV, visible and near infrared," *J. Mod. Opt.* **51**(15), 2315–2322 (2004).
2. S. Pancharatnam, "Achromatic combination of birefringent plates," *Proc. Indiana Acad. Sci.* **XLI**(4), 137 (1955).
3. J. Ma, J. S. Wang, C. Denker, and H. M. Wang, "Optical design of multilayer achromatic waveplate by simulated annealing algorithm," *Chin. J. Astron. Astrophys.* **8**(3), 349–361 (2008).
4. J. M. Herrera-Fernandez, J. L. Vilas, L. M. Sanchez-Brea, and E. Bernabeu, "Design of superachromatic quarter-wave retarders in a broad spectral range," *Appl. Opt.* **54**(33), 9758–9762 (2015).
5. S. Shen, J. She, and T. Tao, "Optimal design of achromatic true zero-order waveplates using twisted nematic liquid crystal," *J. Opt. Soc. Am. A* **22**(5), 961–965 (2005).
6. A. Saha, K. Bhattacharya, and A. K. Chakraborty, "New achromatic quarter-wave combination of birefringent plates," *Opt. Eng.* **51**(1), 013001 (2012).
7. A. Saha, K. Bhattacharya, and A. K. Chakraborty, "Achromatic quarter-wave plate using crystalline quartz," *Appl. Opt.* **51**(12), 1976–1980 (2012).
8. S. B. Powell and V. Gruev, "Calibration methods for division-of-focal-plane polarimeters," *Opt. Express* **21**(18), 21039–21055 (2013).
9. R. M. A. Azzam, "Stokes-vector and Mueller-matrix polarimetry [Invited]," *J. Opt. Soc. Am. A* **33**(7), 1396–1408 (2016).
10. T. Mu, Z. Chen, C. Zhang, and R. Liang, "Optimal design and performance metric of broadband full-Stokes polarimeters with immunity to Poisson and Gaussian noise," *Opt. Express* **24**(26), 29691–29704 (2016).
11. J. Zhang, H. Luo, B. Hui, and Z. Chang, "Image interpolation for division of focal plane polarimeters with intensity correlation," *Opt. Express* **24**(18), 20799–20807 (2016).
12. R. Chipman, "Polarimetry," in *OSA Handbook of Optics* (McGraw-Hill, 2010).
13. K. Adlem, O. L. Parri, D. Wilkes, and C. Topping, "Polymer comprising cyclohexylene groups and its use in films with negative optical dispersion," United States patent US8802813 B2.
14. G. Kang, Q. Tan, X. Wang, and G. Jin, "Achromatic phase retarder applied to MWIR & LWIR dual-band," *Opt. Express* **18**(2), 1695–1703 (2010).
15. X. Deng, F. Liu, J. J. Wang, P. F. Sciortino, Jr., L. Chen, and X. Liu, "Achromatic wave plates for optical pickup units fabricated by use of imprint lithography," *Opt. Lett.* **30**(19), 2614–2616 (2005).
16. H. Kikuta, Y. Ohira, and K. Iwata, "Achromatic quarter-wave plates using the dispersion of form birefringence," *Appl. Opt.* **36**(7), 1566–1572 (1997).
17. D. J. Broer, J. Lub, and G. N. Mol, "Wide-band reflective polarizers from cholesteric polymer networks with a pitch gradient," *Nature* **378**(6556), 467–469 (1995).

18. L. Zhang, M. Wang, L. Wang, D. Yang, H. Yu, and H. Yang, "Polymeric infrared reflective thin films with ultra-broad bandwidth," *Liq. Cryst.* **43**(6), 750–757 (2016).
19. X. Zhao, X. Pan, X. Fan, P. Xu, A. Bermak, and V. G. Chigrinov, "Patterned dual-layer achromatic micro-quarter-wave-retarder array for active polarization imaging," *Opt. Express* **22**(7), 8024–8034 (2014).
20. W. S. Kang, B. J. Mun, G. D. Lee, J. H. Lee, B. K. Kim, H. C. Choi, Y. J. Lim, and S. H. Lee, "Optimal design of quarter-wave plate with wideband and wide viewing angle for three-dimensional liquid crystal display," *J. Appl. Phys.* **111**(10), 103119 (2012).
21. G. Myhre, W. L. Hsu, A. Peinado, C. LaCasse, N. Brock, R. A. Chipman, and S. Pau, "Liquid crystal polymer full-Stokes division of focal plane polarimeter," *Opt. Express* **20**(25), 27393–27409 (2012).
22. W. L. Hsu, G. Myhre, K. Balakrishnan, N. Brock, M. Ibn-Elhaj, and S. Pau, "Full-Stokes imaging polarimeter using an array of elliptical polarizer," *Opt. Express* **22**(3), 3063–3074 (2014).
23. W. L. Hsu, J. Davis, K. Balakrishnan, M. Ibn-Elhaj, S. Kroto, N. Brock, and S. Pau, "Polarization microscope using a near infrared full-Stokes imaging polarimeter," *Opt. Express* **23**(4), 4357–4368 (2015).
24. X. Zhao, A. Bermak, F. Boussaid, and V. G. Chigrinov, "Liquid-crystal micropolarimeter array for full Stokes polarization imaging in visible spectrum," *Opt. Express* **18**(17), 17776–17787 (2010).
25. M. Garcia, S. Gao, C. Edmiston, T. York, and V. Gruev, "A 1300×800 , 700 mW, 30 fps spectral polarization imager," in *Circuits and Systems (ISCAS) 2015 IEEE International Symposium* (IEEE 2015), 1106–1109.
26. X. Tu and S. Pau, "Optimized design of N optical filters for color and polarization imaging," *Opt. Express* **24**(3), 3011–3024 (2016).
27. D. S. Sabatke, M. R. Descour, E. L. Dereniak, W. C. Sweatt, S. A. Kemme, and G. S. Phipps, "Optimization of retardance for a complete Stokes polarimeter," *Opt. Lett.* **25**(11), 802–804 (2000).
28. G. Myhre, A. Sayyad, and S. Pau, "Patterned color liquid crystal polymer polarizers," *Opt. Express* **18**(26), 27777–27786 (2010).
29. S. T. Wu, "Birefringence dispersions of liquid crystals," *Phys. Rev. A Gen. Phys.* **33**(2), 1270–1274 (1986).

1. Introduction

Achromatic polarizers are optical filters that convert one polarization state to another over a broad wavelength range. This type of optical filter serves as an important component for many instruments with applications in photography, spectroscopy, ellipsometry, microscopy, polarimetry, display, and remote sensing, to name a few. In polarization imaging, the achromatic polarizer is a key and necessary component to realize a broadband full-Stokes camera. With a visible achromatic elliptical polarizer, we can measure the polarization of the entire visible spectrum, instead of only at one wavelength. This increases the amount of available light and improves the signal-to-noise-ratio of the measurement. An achromatic elliptical polarizer generally has two components: a retarder and a polarizer. A retarder introduces fixed phase retardance between two orthogonal polarization states, and this retardance is generally wavelength- and temperature- dependent. A polarizer transmits a fixed polarization state and blocks the orthogonal polarization state. An ideal polarizer has low loss for the transmitted state and high extinction ratio. Several designs have been studied for achromatic and superachromatic quarter-wave and half-wave retarders using multi-layer films [1–7]. In this paper, we consider the problem of designing an achromatic elliptical polarizer of arbitrary ellipticity. The achromatic elliptical polarizer consists of a multi-layer retarder and an achromatic polarizer, which can be either a linear or circular polarizer. In section 2, the design of the retarder using a multi-layer configuration is presented. For a two-layer retarder, the design problem has a simple geometric interpretation of finding two overlapping arcs on the Poincaré sphere. In section 3, the technique is applied to the design of elliptical polarizers that operate in the visible spectrum and can be used in an optimized polarimeter. It is shown that our achromatic elliptical polarizer design can be applied in existing polarimetry techniques [8–11] and provide a solution to full-Stokes measurement of broadband light. In section 4, the fabrication and testing of the achromatic elliptical polarizer are presented. The measured performance of the polarizer is compared with the theoretical calculation. In the final section, generalization of the technique to better performance by addition of retarder layer is discussed, with particular emphasis on flatter wavelength response and larger operating wavelength range.

2. Theory of achromatic elliptical polarizers

In this section, we discuss the theory of designing an achromatic elliptical polarizer. By definition, analyzers are polarization elements that transmit a desired polarization state in maximum transmittance, while polarizers are polarization elements that generate a desired polarization state [12]. There are three main approaches to making an achromatic elliptical polarizer. One approach uses negative dispersion materials [13] or form birefringence [14–16] to reduce the variation of retardance due to the wavelength change. Another approach uses helical materials with variable pitch, such as cholesteric liquid crystal polymer, to achieve a broadband circular polarizer [17,18]. This method is generally applicable to circular polarization only. The topic of this paper is the third approach, which utilizes a combination of multi-layer retarders and one polarizer to form an achromatic elliptical polarizer. Similar techniques have been applied to the design of achromatic circular polarizers [19,20], but our design is applicable to any elliptical polarization with arbitrary ellipticity. Thus, our technique is more general and can be applied to a broader range of applications.

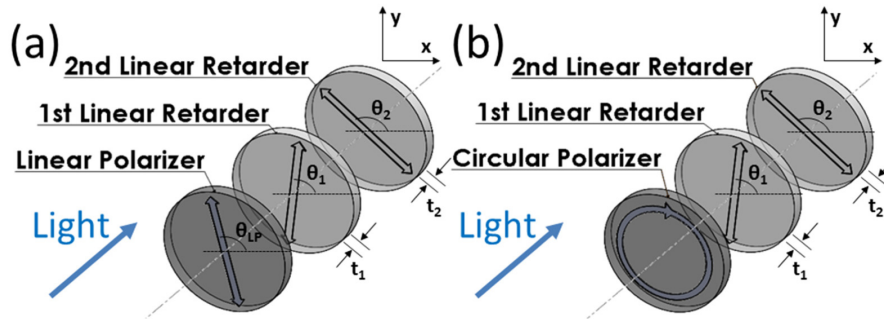


Fig. 1. The schematics of an achromatic elliptical polarizer are shown with (a) a linear polarizer and with (b) a circular polarizer.

Figure 1 shows our design schematics of a unidirectional, achromatic elliptical polarizer. A bidirectional achromatic elliptical polarizer can be made by adding two similar retarder layers in front of the polarizer. Our design consists of two linear retarders and one achromatic linear or circular polarizer. The input light first passes the achromatic polarizer, which generates either linear or circular polarized light. The light then passes the two linear retarders, resulting in an elliptical polarized light. In general, each linear retarder has a different retardance but a fixed fast-axis orientation for different wavelength. By using two linear retarders, we show how to compensate for this variability and make the output polarization state nearly achromatic, in other words, as close as possible to the target elliptical polarization state. We apply our theory to an achromatic polarizer design for the visible band ($\lambda = 450\text{nm}$ to 650nm). As the figure of merit of the performance of the achromatic elliptical polarizer, we use the following deviation function,

$$\|s(\lambda) - s_{\text{target}}\|_m = \max \left(\sqrt{(s_1(\lambda) - \cos(2\varepsilon))^2 + s_2(\lambda)^2 + (s_3(\lambda) - \sin(2\varepsilon))^2} \right) \quad (1)$$

$$450\text{nm} \leq \lambda \leq 650\text{nm}$$

where $s(\lambda) = [s_1(\lambda), s_2(\lambda), s_3(\lambda)] = [S_1(\lambda)/S_0(\lambda), S_2(\lambda)/S_0(\lambda), S_3(\lambda)/S_0(\lambda)]$ contains the last three components of the normalized Stokes vector of the achromatic elliptical polarizer output state at the wavelength λ , and $S_{0,1,2,3}(\lambda)$ are the Stokes vector. $s_{\text{target}} = [\cos(2\varepsilon), 0, \sin(2\varepsilon)]$ contains the last three components of the normalized Stokes vector of the target elliptical polarization with ellipticity ε .

The operation of a linear retarder in converting polarization states can be understood geometrically. If we represent the input polarization state and output polarization state by points on the Poincaré sphere, then the output point can be obtained by rotating the input

point about vector $[\cos(2T), \sin(2T), 0]$ by R degree, where T is the fast-axis angle with respect to the horizontal axis, and R is the retardance of the linear retarder. This behavior is illustrated in Fig. 2. An input broadband polarized light through a linear retarder forms an arc on the Poincaré sphere.

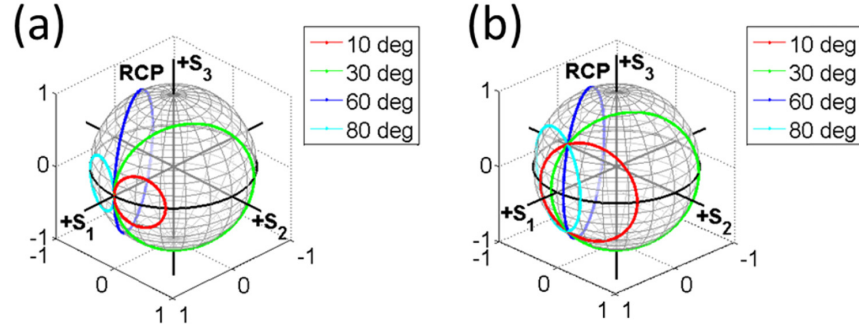


Fig. 2. The schematics show the trajectory of the output state on the Poincaré sphere, when the input state passes through a linear retarder with fixed fast-axis orientation but varying retardances from 0 to 360 degrees. Each trajectory represents a different fast-axis orientation

T . The input state is (a) $s = [1, 0, 0]$ and (b) $s = [\sqrt{2/3}, 0, \sqrt{1/3}]$.

We divide our analysis into two cases. In the first case, we consider the configuration of an achromatic elliptical polarizer using one linear polarizer and two linear retarders as shown in Figs. 1(a) and 3(a). The first retarder rotates the linear polarized (LP) light to Arc A. Considering the reverse direction, we see that the second retarder rotates the target state to Arc B. The length of the arcs is determined by the wavelength range. If both Arc A and Arc B exactly overlap each other, then the second retarder rotates Arc A back to the target point perfectly, and an achromatic elliptical polarizer is achieved. Geometrically, the two arcs can be nearly overlapping if they are tangent and bent in the same direction. This coincidence can be further improved by slightly shifting one arc toward the other. Once the gap between the midpoints of two arcs is equal to the gap between the endpoints, a maximal coincidence is achieved.

We observe in Fig. 2 that all circles are centered on the equatorial plane. Hence, these circles can only be tangent at the equator. Therefore, we can make the conclusion that the midpoints of Arc A and Arc B are both located at the equator. Based on this, the optimized design for the achromatic elliptical polarizer can be calculated in the following way. First, we define the unit thickness of one linear retarder as a retardance range of $180 - \delta$ to $180 + \delta$ degrees in the visible band ($\lambda = 450\text{nm}$ to 650nm), where δ depends on the material's optical properties. Since the first retarder layer rotates the LP state, which is on the equator, to an arc, whose midpoint is also on the equator, the relative thickness of the first layer, t_1 , is equal to 1. The actual thickness depends on the material properties, which in our experiment are measured by a polarimeter, and is equal to the thickness of a retarder with an average retardance of 180 over the wavelength range of interest. Similarly, the second layer translates the target state into an arc, whose midpoint is also on the equator. Thus, the relative thickness of the second layer, t_2 , is equal to $\beta/180^\circ$, where β is the rotation angle to rotate the target state to the equator. Figure 3(a) shows a schematic of Arc A and Arc B on the Poincaré sphere.

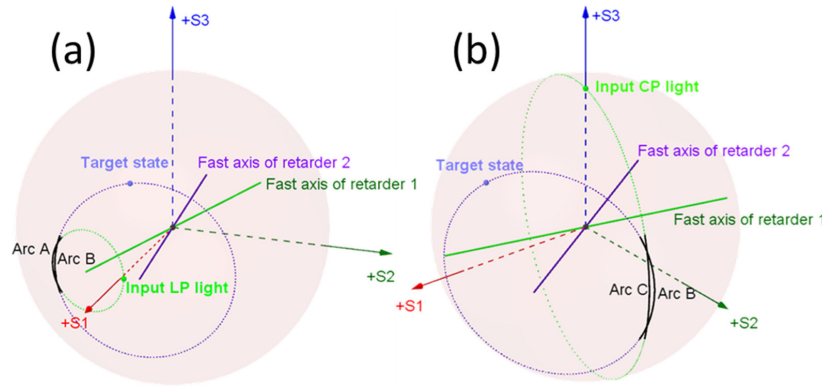


Fig. 3. The geometry of overlapping arcs on a Poincaré sphere is shown for (a) an input state of linear polarized light and (b) an input state of circular polarized light

In 3D space, a circle of radius r centered at point \vec{C} can be described by a parametric equation:

$$\vec{P}(t) = r \cos(t) * \vec{u} + r \sin(t) * (\vec{n} \times \vec{u}) + \vec{C} \quad (2)$$

Here, \vec{n} is the unit normal vector to the plane of circle, and \vec{u} is any unit vector perpendicular to \vec{n} , in other words, any unit vector on the plane of the circle. The parameter, t , is the angle between the line \vec{CP} and the unit vector, \vec{u} . The values of \vec{n} , \vec{u} , \vec{C} , r and t for Arc A and B are given below. Here $\theta_{1,2}$ and $t_{1,2}$ are the fast-axis orientation and thickness of the two retarder layers, and $m_{1,2}$ are the distances from the origin to the centers of curvature of the two arcs.

$$\begin{aligned} \vec{n}_A &= [\cos(2\theta_1), \sin(2\theta_1), 0], \vec{u}_A = [-\sin(2\theta_1), \cos(2\theta_1), 0] \\ \vec{C}_C &= [m_1 * \cos(2\theta_1), m_1 * \sin(2\theta_1), 0], r_C = \sqrt{1-m_1^2}, 180 - \delta < t_A < 180 + \delta \\ \vec{n}_B &= [\cos(2\theta_2), \sin(2\theta_2), 0], \vec{u}_B = [-\sin(2\theta_2), \cos(2\theta_2), 0] \\ \vec{C}_B &= [m_2 * \cos(2\theta_2), m_2 * \sin(2\theta_2), 0], r_B = \sqrt{1-m_2^2}, 180 - t_2\delta < t_B < 180 + t_2\delta \end{aligned} \quad (3)$$

Note that the m_i can be derived from θ_{LP} , which is the angle of the linear polarizer's transmission axis respect to the horizontal.

$$\theta_{LP} = \theta_i + \cos^{-1}(m_i) / 2 \quad (4)$$

Combining Eq. (2) and Eq. (3), we can find the coordinates of the midpoints and endpoints of two arcs. The coordinates of the midpoints of Arc A and Arc B are given by

$$\begin{aligned} \vec{P}_A(180) &= [\sqrt{1-m_1^2} \sin(2\theta_1) + m_1 \cos(2\theta_1), -\sqrt{1-m_1^2} \cos(2\theta_1) + m_1 \sin(2\theta_1), 0] \\ \vec{P}_B(180) &= [\sqrt{1-m_2^2} \sin(2\theta_2) + m_2 \cos(2\theta_2), -\sqrt{1-m_2^2} \cos(2\theta_2) + m_2 \sin(2\theta_2), 0] \end{aligned} \quad (5)$$

The coordinates of the endpoints of Arc A and Arc B are given by

$$\begin{aligned} \vec{P}_A(180 - \delta) &= [\sqrt{1-m_1^2} \cos(\delta) \sin(2\theta_1) + m_1 \cos(2\theta_1), \\ &\quad -\sqrt{1-m_1^2} \cos(\delta) \cos(2\theta_1) + m_1 \sin(2\theta_1), \sqrt{1-m_1^2} * \sin(\delta)] \\ \vec{P}_B(180 - t_2\delta) &= [\sqrt{1-m_2^2} \cos(t_2\delta) \sin(2\theta_2) + m_2 \cos(2\theta_2), \\ &\quad -\sqrt{1-m_2^2} \cos(t_2\delta) \cos(2\theta_2) + m_2 \sin(2\theta_2), \sqrt{1-m_2^2} \sin(t_2\delta)] \end{aligned} \quad (6)$$

The midpoints and endpoints are all on the unit sphere, and the dot product of two points is a good figure of merit of the amount of gap between the two points.

$$\begin{aligned}\vec{P}_A(180) \bullet \vec{P}_B(180) &= (\sqrt{1-m_1^2} \sqrt{1-m_2^2} + m_1 m_2) \cos[2(\theta_1 - \theta_2)] \\ &\quad + (\sqrt{1-m_1^2} m_2 - \sqrt{1-m_2^2} m_1) \sin[2(\theta_1 - \theta_2)] \\ \vec{P}_A(180 - \delta) \bullet \vec{P}_B(180 - t_2 \delta) &= (\sqrt{1-m_1^2} \sqrt{1-m_2^2} \cos(\delta) \cos(t_2 \delta) + m_1 m_2) \cos[2(\theta_1 - \theta_2)] \\ &\quad + \sqrt{1-m_1^2} \sqrt{1-m_2^2} \sin(\delta) \sin(t_2 \delta) \\ &\quad + (\sqrt{1-m_1^2} m_2 \cos(\delta) - \sqrt{1-m_2^2} m_1 \cos(t_2 \delta)) \sin[2(\theta_1 - \theta_2)]\end{aligned}\quad (7)$$

When Arc A and Arc B achieve maximal coincidence, the gap between midpoints should be equal to the gap between endpoints. Hence, in the case of maximal coincidence, the two dot products are equal.

$$\vec{P}_A(180 - \delta) \bullet \vec{P}_B(180 - t_2 \delta) = \vec{P}_A(180) \bullet \vec{P}_B(180) \quad (8)$$

Combining Eq. (7) and Eq. (8), we have

$$\frac{1 - \cos(\delta) \cos(t_2 \delta)}{\tan[2(\theta_1 - \theta_2)]} - \frac{\sin(\delta) \sin(t_2 \delta)}{\sin[2(\theta_1 - \theta_2)]} = \frac{m_1(1 - \cos(t_2 \delta))}{\sqrt{1-m_1^2}} - \frac{m_2(1 - \cos(\delta))}{\sqrt{1-m_2^2}} \quad (9)$$

Note that both t_2 and m_2 can be calculated from θ_2 by simple geometric derivation.

$$\begin{aligned}m_2 &= \cos(2\varepsilon) \cos(2\theta_2) \\ t_2 &= \cot^{-1}(\cot(2\varepsilon) \sin(2\theta_2)) / 180\end{aligned}\quad (10)$$

Combining the Eq. (9) and Eq. (10), m_1 can be expressed in terms of θ_1 and θ_2 . Therefore, the dot product of the two midpoints is a function of only θ_1 and θ_2 .

$$\vec{P}_A(180) \bullet \vec{P}_B(180) = G(\theta_1, \theta_2) \quad (11)$$

$G(\theta_1, \theta_2)$ is a function of the two fast-axis angles and has multiple local maximums. Our goal is to find the two arcs with the most overlap, and the solution of the problem can be found by maximizing $G(\theta_1, \theta_2)$. The expression for $G(\theta_1, \theta_2)$ is complicated and difficult to maximize analytically; however, the solution can be easily solved numerically by using MATLAB optimization toolbox. The only parameter in the optimization is δ , which depends on material properties of the linear retarders. Once θ_1 and θ_2 are determined, t_2 can be calculated using Eq. (9), and θ_{LP} can be calculated using Eq. (4), Eq. (9) and Eq. (10).

We next consider the second case for the configuration of achromatic elliptical polarizers using one circular polarizer and two linear retarders as shown in Figs. 1(b) and 3(b). For this case, the first retarder rotates the circular polarized (CP) light to Arc C. Considering the reverse direction, we see that the second retarder rotates the target state to Arc B. The problem becomes maximizing the coincidence of Arc B and Arc C. Since the first retarder layer rotates the CP state, which is on the pole, to Arc C, of which the midpoint is on the equator, the rotation angle of the midpoint is 90 degrees, and the relative thickness is equal to 1/2. The relative thickness of the second retarder layer t_2 is equal to $\beta/180^\circ$, which is the same as the first case. Figure 3(b) shows a schematic of Arc C and Arc B on the Poincaré sphere. For Arc C, the values of \vec{n} , \vec{u} , \vec{C} , r_C and t_C are given as follows:

$$\begin{aligned}\vec{n}_C &= [\cos(2\theta_1), \sin(2\theta_1), 0], \vec{u}_C = [0, 0, 1] \\ \vec{C}_C &= [0, 0, 0], r_C = 1, 90 - \delta/2 < t_C < 90 + \delta/2\end{aligned}\quad (12)$$

From Eq. (12), we can find the coordinates of the midpoints and endpoints of Arc C. The coordinate of the midpoint of arc C is given by

$$\vec{P}_C(90) = [\sin(2\theta_1), -\cos(2\theta_1), 0] \quad (13)$$

The coordinate of the endpoint of Arc C is given by

$$\vec{P}_C(90 - \delta/2) = [\cos(\delta/2)\sin(2\theta_1), -\cos(\delta/2)\cos(2\theta_1), \sin(\delta/2)] \quad (14)$$

The dot products of midpoints and endpoints are

$$\begin{aligned} \vec{P}_C(90) \cdot \vec{P}_B(180) &= \sqrt{1-m_2^2} \cos[2(\theta_1 - \theta_2)] + m_2 \sin[2(\theta_1 - \theta_2)] \\ \vec{P}_C(90 - \delta/2) \cdot \vec{P}_B(180 - t_2\delta) &= \sqrt{1-m_2^2} \cos(\delta/2) \cos(t_2\delta) \cos[2(\theta_1 - \theta_2)] \\ &\quad + \sqrt{1-m_2^2} \sin(\delta/2) \sin(t_2\delta) \\ &\quad + m_2 \cos(\delta/2) \sin[2(\theta_1 - \theta_2)] \end{aligned} \quad (15)$$

When the two dot products are equal, we obtain the following equation:

$$\frac{m_2}{\sqrt{1-m_2^2}} = \frac{(1 - \cos \frac{\delta}{2} \cos(t_2\delta)) \cos[2(\theta_1 - \theta_2)] - \sin \frac{\delta}{2} \sin(t_2\delta)}{(\cos \frac{\delta}{2} - 1) \sin[2(\theta_1 - \theta_2)]} \quad (16)$$

Since both t_2 and m_2 can be derived from θ_2 , using Eq. (10), Eq. (16) is simply a relation between θ_2 and $\Delta\theta = \theta_1 - \theta_2$, and it can be rewritten in a simpler form to solve $\Delta\theta$ from θ_2 .

$$a(\theta_2) \cos[2\Delta\theta] + b(\theta_2) \sin[2\Delta\theta] = c(\theta_2) \quad (17)$$

Here, coefficients a , b and c are all functions of θ_2 .

$$\begin{aligned} a(\theta_2) &= 1 - \cos \frac{\delta}{2} \cos(t_2\delta) \\ b(\theta_2) &= \frac{m_2}{\sqrt{1-m_2^2}} (1 - \cos \frac{\delta}{2}) \\ c(\theta_2) &= \sin \frac{\delta}{2} \sin(t_2\delta) \end{aligned} \quad (18)$$

The solution of this equation is

$$\begin{aligned} \Delta\theta &= \frac{\sin^{-1}(\frac{c}{\sqrt{a^2+b^2}}) - \phi}{2} \\ [\sin \phi, \cos \phi] &= [\frac{a}{\sqrt{a^2+b^2}}, \frac{b}{\sqrt{a^2+b^2}}] \end{aligned} \quad (19)$$

Similarly, by combining Eq. (15) and Eq. (19), we find that the dot product of the two midpoints is a function of only θ_2 .

$$\vec{P}_A(180) \cdot \vec{P}_B(180) = H(\theta_2) \quad (20)$$

As in the previous case, the problem now becomes one of maximizing $H(\theta_2)$. Once the optimized θ_2 is determined, θ_1 can be derived using Eq. (19), and t_2 can be derived using Eq. (10). After we have the optimized values of θ_1 , θ_2 , t_1 , t_2 and θ_{LP} , we can assemble an achromatic elliptical polarizer using the retarder and polarizer layers with the calculated optimized angles and thicknesses.

3. Application of achromatic elliptical polarizer to broadband full-Stokes imaging

Full-Stokes imaging records the polarization property of objects and has a variety of applications including biomedical imaging, remote sensing, and space exploration. There have been many approaches to the design of full-Stokes camera [21–25]. Many of these approaches are limited to one wavelength, such that the camera cannot record the polarization of different colors simultaneously. One reason for this limitation is the lack of achromatic circular and elliptical analyzers, which are necessary to record the information of all components of the Stokes vector. The transmitted flux of an elliptical analyzer depends on the fraction of the desired elliptical polarization in incident light. The principle of a full-Stokes camera is to capture the polarization property of an object by measuring the intensity response of the incident light through different analyzers. To design a broadband full-Stokes camera, achromatic elliptical analyzers are often required. In this section, the relationship between achromatic elliptical polarizers and broadband full-Stokes imaging are discussed. To achieve full-Stokes imaging, a minimum of four intensity measurements through four different elliptical analyzers is required. The relationship between the four intensity measurements $[I_0, I_1, I_2, I_3]$ and the input Stokes vector $S = [S_0, S_1, S_2, S_3]$ can be described as

$$\begin{bmatrix} I_0 \\ I_1 \\ I_2 \\ I_3 \end{bmatrix} = W \begin{bmatrix} S_0 \\ S_1 \\ S_2 \\ S_3 \end{bmatrix} \quad (21)$$

Here, W is the so-called measurement matrix, and it is the combination of the first row of the Mueller matrix of each elliptical analyzer. In the broadband full-stokes imaging, the measurement matrix needs to be achromatic. Therefore, for each elliptical analyzer, the first row of its Mueller matrix needs to be achromatic. We assume that the elliptical analyzers are made by a series of linear retarders followed by a linear polarizer. The incident light first transmits through these linear retarders and then through the linear polarizer. The Mueller Matrix can be calculated as follows:

$$M_{analyzer} = M_{LP}(\theta_{LP})M_{LR}(\delta_N, \theta_N) \cdots M_{LR}(\delta_2, \theta_2)M_{LR}(\delta_1, \theta_1) \quad (22)$$

where $M_{LP}(\theta)$ represents the Mueller matrix of a linear polarizer, which has its transmission axis oriented at an angle θ with respect to horizontal. $M_{LR}(\delta, \theta)$ represents the Mueller matrix of a linear retarder, which has its fast axis oriented at an angle θ with respect to the horizontal and its retardance equal to δ . The two Mueller matrices are given by

$$M_{LR}(\delta, \theta) = \begin{bmatrix} 1 & 0 & 0 & 0 \\ 0 & \cos^2(2\theta) + \sin(2\theta)\cos(2\theta)\sin(\delta) & \sin(2\theta)\cos(2\theta)(1 - \cos(\delta)) & \sin(2\theta)\sin(\delta) \\ 0 & \cos(\delta)\sin^2(2\theta) & (1 - \cos(\delta))\sin(2\theta)\cos(2\theta) & -\cos(2\theta)\sin(\delta) \\ 0 & (1 - \cos(\delta))\sin(2\theta)\cos(2\theta) & \sin^2(2\theta)\cos(\delta) & \cos(\delta)\cos(2\theta) \end{bmatrix} \quad (23)$$

$$M_{LP}(\theta) = \frac{1}{2} \begin{bmatrix} 1 & \cos(2\theta) & \sin(2\theta) & 0 \\ \cos(2\theta) & \cos^2(2\theta) & \sin(2\theta)\cos(2\theta) & 0 \\ \sin(2\theta) & \sin(2\theta)\cos(2\theta) & \sin^2(2\theta) & 0 \\ 0 & 0 & 0 & 0 \end{bmatrix}$$

The transpose of Eq. (23) is

$$\begin{aligned}
 M_{\text{analyzer}}^T &= M_{LR}^T(\delta_1, \theta_1) M_{LR}^T(\delta_2, \theta_2) \cdots M_{LR}^T(\delta_N, \theta_N) M_{LP}^T(\theta_{LP}) \\
 &= M_{LR}(\delta_1, \theta_1 + \pi/2) M_{LR}(\delta_2, \theta_2 + \pi/2) \cdots M_{LR}(\delta_N, \theta_N + \pi/2) M_{LP}(\theta_{LP})
 \end{aligned} \quad (24)$$

We find that the transposition of the analyzer's Mueller matrix is actually a linear polarizer followed by a series of linear retarders, which is an elliptical polarizer. Realizing that the first row of the analyzer is achromatic, the first column of the transposed matrix is also achromatic. In other words, the polarizance of the elliptical polarizer is achromatic, which makes the polarizer an achromatic elliptical polarizer. Once we have an achromatic elliptical polarizer made by a linear polarizer followed by a series of linear retarders, we can rotate each retarder by $\pi/2$, reverse the order of the polarizer and retarders, and finally get an achromatic elliptical analyzer which has an achromatic first row in its Mueller matrix. The analyzer can be then applied to a broadband full-Stokes camera.

Figure 4(a) shows the four elliptical polarizers adopted for our broadband full-Stokes camera design. The advantage of this design is that the four elliptical polarizers form a tetrahedron on the Poincaré sphere, which minimizes the measurement noise [26, 27]. Another advantage of this design is that the four elliptical polarizers are symmetrical and can be fabricated by conventional photoalignment technique [28]. The elliptical polarizer (EP) can be made by combining one linear polarizer and two linear retarders. Once we have the first elliptical polarizer (EP1), the second elliptical polarizer (EP2) can be obtained by rotating EP1 by 90 degrees. The third and fourth elliptical polarizer (EP3 and EP4) can be obtained by first flipping each layer of EP1 around the horizontal and then rotating it by ± 45 degrees. The four elliptical polarizers can be combined to form a 2×2 macro pixel in a division of focal plane (DoFP) configuration as shown in Fig. 4(b).

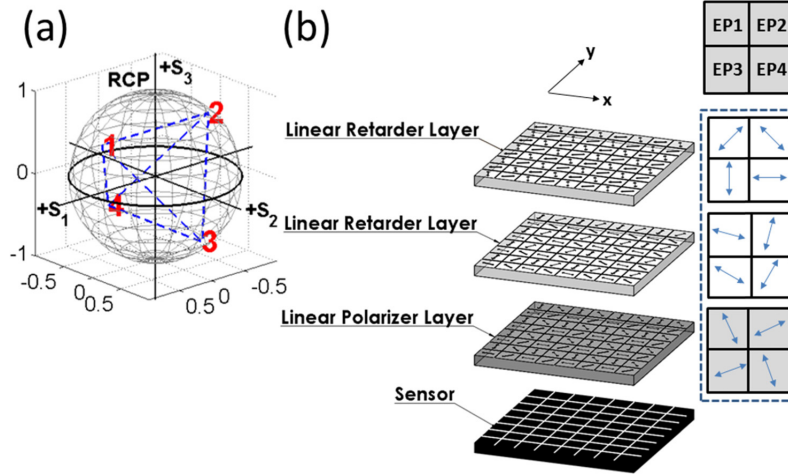


Fig. 4. (a) The regular tetrahedron adopted for a broadband full-Stokes camera is shown along with the Poincaré sphere. The coordinates of vertices 1, 2, 3, 4 are $[\sqrt{2/3}, 0, \sqrt{1/3}]$, $[-\sqrt{2/3}, 0, \sqrt{1/3}]$, $[0, \sqrt{2/3}, -\sqrt{1/3}]$, $[0, -\sqrt{2/3}, -\sqrt{1/3}]$ respectively. (b) A design of a DoFP broadband full-Stokes camera shows the array of four elliptical polarizers. The macro pixel of each layer is displayed on right.

4. Fabrication and optical characterization of an achromatic elliptical polarizer

In this section, we describe the process of fabricating an achromatic elliptical polarizer using liquid crystal polymer (LCP) as the retarder layer. The LCP is RMM141C reactive mesogen manufactured by EMD Chemicals. The LCP is photo-aligned using ultraviolet light (UV) and a linearly photopolymerizable polymer ROP108 (LPP) made by Roloc Technologies to form a linear retarder layer. Figure 5(a) shows the retardance curve of RMM141C (17% weight-to-

weight ratio in toluene and spin coating at 8000rpm) as a function of wavelength. This retardance curve can be fit to the measurement results by using a theoretical retardance equation of LCP derived from a single-band birefringence dispersion model [29].

$$\Delta\phi(t, \lambda) = \frac{2\pi t}{\lambda} \Delta n = Ct \frac{\lambda \lambda^{*2}}{\lambda^2 - \lambda^{*2}} \quad (25)$$

Here, $\Delta\phi$ is the retardance, Δn is the birefringence, C is a proportionality constant, t is the thickness, λ is the wavelength, and λ^* is the mean resonance frequency of the band.

Utilizing the measured retardance curve, the optimized achromatic elliptical polarizer, i.e. EP1, is found to have the following parameters: $\theta_1 = 82.76^\circ$, $\theta_2 = 3.48^\circ$, $t_1 = 1$, $t_2 = 0.446$, $\theta_{LP} = 0.63^\circ$. Here $t_1 = 1$ means that the film thickness satisfies the relation $\Delta\phi(\lambda = 450\text{nm}) + \Delta\phi(\lambda = 650\text{nm}) = 2\pi$.

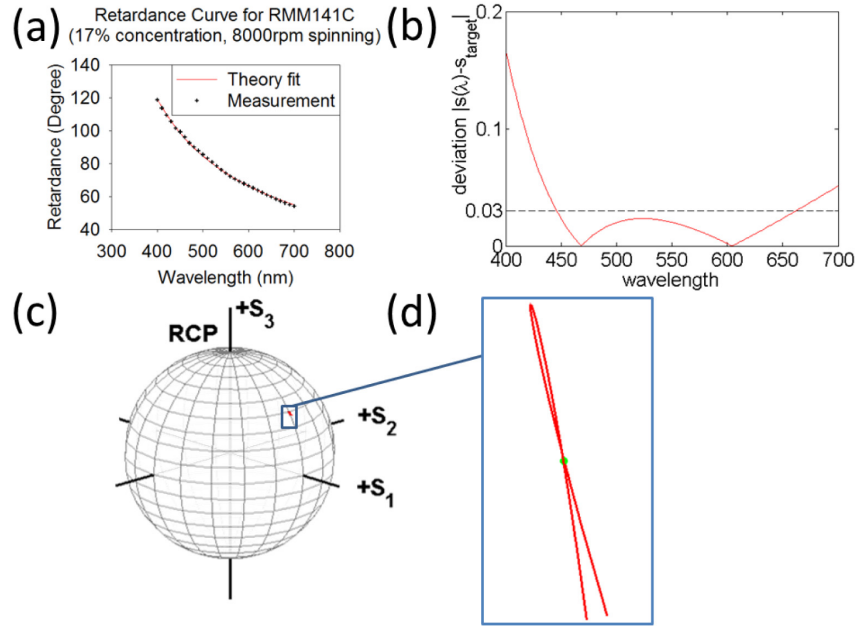


Fig. 5. (a) The retardance curve of liquid crystal polymer RMM141C is plotted as a function of wavelength. (b) The plot shows the deviation curve of the optimized achromatic elliptical polarizer made of RMM141C. (c) The curve of the optimized achromatic elliptical polarizer output state on the Poincaré sphere is shown for wavelength range from 450nm to 650nm; (d) The magnified view of (c) is shown. The green dot is the target state.

Figure 5(b) shows the deviation curve of the optimized achromatic elliptical polarizer. The deviation is defined as the absolute value of the difference between the last three components of the normalized Stokes vector of the achromatic polarizer's output state and the last three components of the normalized Stokes vector of the target elliptical polarization state. Figure 5(c) shows the trajectory of the output polarization state on the Poincaré sphere. The detail of the trajectory is shown in Fig. 5(d).

Figure 6 shows a schematic diagram of the fabrication process of the achromatic elliptical polarizer. The fabrication process consists of three parts: (1) fabrication of the second retarder, (2) fabrication of the first retarder, and (3) integration of retarders with a wire-grid linear polarizer. The two retarders are made by LCP and LPP on a glass substrate. The broadband wire grid linear polarizer is a laminated film manufactured by Asahi Kasei (model WGF). Detailed steps are described below.

- 1) The LPP is spin coated on soda lime glass substrate at 2500rpm for one minute. The glass substrate is 1.5 inches in diameter and has a flat cut on the edge to help with the angle alignment.
- 2) The substrate is hard baked at 170 °C for 5 minutes and exposed under 10mW UV light at 365nm for 10 minutes with a UV linear polarizer on top in order to produce linearly polarized UV illumination (LPUV). The linear polarized UV light defines the fast-axis orientation of LCP.
- 3) The LCP solution is made by adding RMM141C to toluene at a 17% weight-to-weight ratio and then spin coated at 8000rpm for 30 seconds. The LCP aligns with the LPP and forms a linear retarder layer. The fast-axis orientation is defined by the orientation of anisotropically cross-linked LPP.
- 4) The substrate is hard baked at 53 °C for 5 minutes and exposed with 10mW UV light at 365nm for 2 minutes to cure the LCP.
- 5) A 50nm silicon oxide layer is deposited onto the substrate using electron beam evaporation technique. The silicon oxide layer is used as isolation between the two linear retarder layers. The silicon oxide layer appears to reduce the retardance of the thin film by about 3 percent.
- 6) The sample is characterized by an Axometrics polarimeter. A re-optimization is performed to determine the best fast-axis orientation for the second retarder layer based on the measured retardance.
- 7) Steps 1 to 5 are repeated for the fabrication of the first retarder layer. The LCP solution for the first retarder is made by adding RMM141C to toluene at a 30% weight-to-weight ratio. The LCP solution is spin coated at 4000rpm for 30 seconds.
- 8) A wire grid linear polarizer film is oriented and put in the front of the two retarder layers.

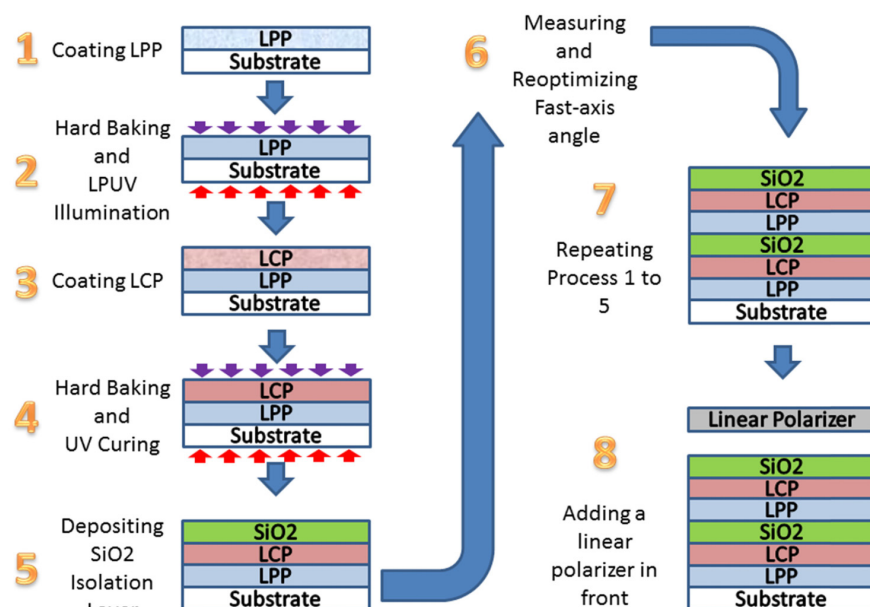


Fig. 6. The schematic shows the fabrication process of an achromatic elliptical polarizer.

The sample is characterized by an Axometrics Mueller matrix polarimeter. Figure 7(a) shows the deviation curve of the sample and the comparison to the theoretical curve predicted by the optimization. The experimental result and theory prediction match well within measurement errors. Figure 7(b) shows the trajectory of the sample's output state on the Poincaré sphere. Figure 7(c) shows the magnified view of the experimental curve. The sample has a maximum deviation of about 4% at for wavelength of 450nm to 650nm, which makes it a good achromatic elliptical polarizer.

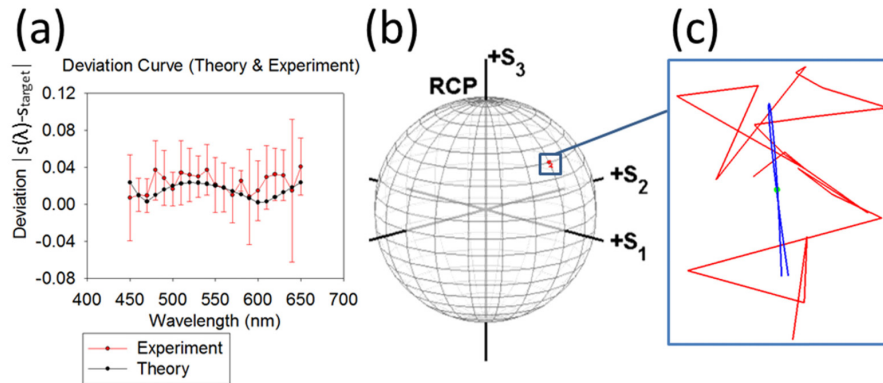


Fig. 7. (a) A comparison of the deviation curve of the fabricated sample and theoretical prediction is shown. The bar represents the measurement error of the Axometrics polarimeter. (b) The trajectory of the sample's output state is shown on the Poincaré sphere for wavelength range from 450nm to 650nm. (c) The magnified view of the trajectory in (b). The blue curve is the trajectory of theoretical prediction. The green dot is the target state.

5. Discussion and conclusion

In this paper, a general theory of achromatic elliptical polarizers is presented. A sample consists of two-layer retarder and one-layer polarizer is fabricated and tested with performance agreed well with our calculation. A better performance of achromatic elliptical polarizer, i.e. a flatter wavelength response, can be achieved by adding a third retarder layer or additional retarder layers. In this case, the first retarder layer and the last retarder layer rotate the input state and the target state to an input arc and an output arc, respectively, and the remaining retarder layer or layers can be understood as transformations of arcs. These transformations should transform the input arc to a curve that matches the output arc. With addition of more retarder layers, more degrees of freedom are introduced, reducing the difference between the input and output arcs and resulting in a flatter wavelength response and a larger operating wavelength range. In this final section, we explore the theoretical performance of achromatic elliptical polarizer with more than two retarder layers.

MATLAB optimization toolbox is used to find the optimized design of three-layer retarder and four-layer retarder configuration, for visible band ($\lambda = 450\text{nm}$ to 650nm) and a wider band ($\lambda = 400\text{nm}$ to $1\mu\text{m}$). The material for the retarder layer and the target state are the same as that in section 4. For three-layer and four-layer configurations, geometrical analysis is so complicated that the number of optimization variables cannot be reduced into one or two, as in the case of the two-layer configuration. Instead, we directly optimize the thickness and fast-axis orientation for all retarder layers using the MATLAB optimization toolbox. Although we have performed the calculation using many iterations, we cannot ascertain that the results are the global minimum. The optimization results are likely to be local minimum, but they provide a general trend for addition of retarder layers and a good set of designs with low deviation. Figure 8 shows the deviation curves of two-layer, three-layer and four-layer configuration. For visible band, the maximum deviation is reduced from 2.3% to 0.3% and 0.04% by using three-layer and four-layer configuration, respectively. When the operating

wavelength increases from 650nm to 1 μ m, the two-layer configuration has a high deviation of 12%, while the three-layer and four-layer have a better performance, with maximum deviation of 1% and 0.7%, respectively. Our calculations show the general trend that additional layers of retarder can flatten the deviation and increase the operating wavelength range of the achromatic elliptical polarizer.

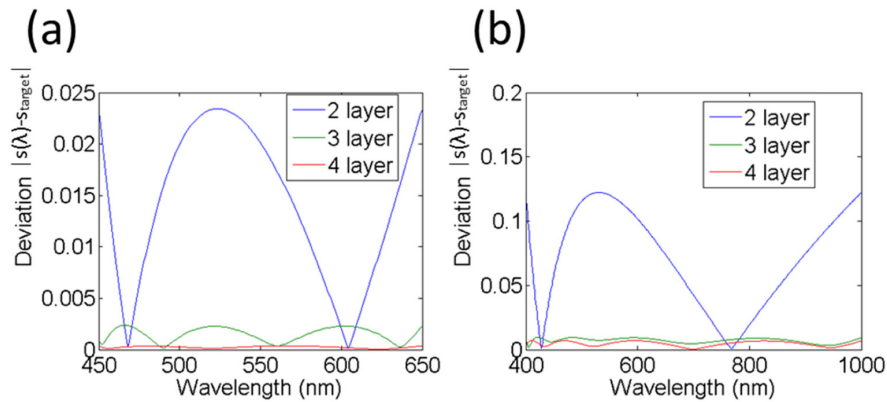


Fig. 8. The deviation curve of optimized 2, 3, 4 retarder layer configurations for wavelength range of (a) $\lambda = 450\text{nm}$ to 650nm and (b) $\lambda = 400\text{nm}$ to $1\mu\text{m}$.

In conclusion, we present one design approach for the achromatic elliptical polarizer and apply our design to broadband full-Stokes imaging. The achromatic elliptical polarizer is comprised of a minimum of two linear retarders and one linear or circular polarizer. Our technique can be applied to the design of polarizer of any ellipticity, including circular polarization.

Funding

Arizona Technology Research Infrastructure Fund (TRIF); National Science Foundation (NSF) (1607358).

Acknowledgments

The authors thank Prof. Russell Chipman for the use of his laboratory equipment, Jeffrey Davis for help on the fabrication process, and Barry Seff at EMD Performance Materials and Dr. David Wilkes at Merck KGaA for help on reactive mesogens.